

1        **A New Aerosol Dry Deposition Model for Air Quality and Climate Modeling**

2

3        Jonathan E. Pleim<sup>1</sup>, Limei Ran<sup>2</sup>, Rick D. Saylor<sup>3</sup>, Jeff Willison<sup>4</sup>, and Francis S.

4        Binkowski<sup>5</sup>

5

6        <sup>1</sup>U.S. Environmental Protection Agency, Research Triangle Park, North Carolina, USA,

7        pleim.jon@epa.gov

8        <sup>2</sup>U.S. Department of Agriculture, Natural Resources Conservation Service, Greensboro,

9        North Carolina, USA, limei.ran@usda.gov

10       <sup>3</sup>Air Resources Laboratory, National Oceanic and Atmospheric Administration, Oak

11       Ridge, Tennessee, USA, [rick.saylor@noaa.gov](mailto:rick.saylor@noaa.gov)

12       <sup>4</sup>U.S. Environmental Protection Agency, Research Triangle Park, North Carolina, USA,

13       willison.jeffrey@epa.gov

14       <sup>4</sup>Institute for the Environment, University of North Carolina at Chapel Hill, Chapel Hill,

15       North Carolina, USA, francisbinkowski@gmail.com

16

17       **Key Points**

18       • New aerosol deposition velocity model agrees better with observations than

19       current models

20       • Impaction on microscale obstacles such as leaf hairs is key process

21       • New aerosol deposition velocity model increases dry deposition of PM<sub>2.5</sub>

22

23

24

25

26

27 **Abstract**

28 Dry deposition of aerosols from the atmosphere is an important but poorly understood  
29 and inadequately modeled process in atmospheric systems for climate and air quality.  
30 Comparisons of currently used aerosol dry deposition models to a compendia of  
31 published field measurement studies in various landscapes show very poor agreement  
32 over a wide range of particle sizes. In this study, we develop and test a new aerosol dry  
33 deposition model that is a modification of the current model in the Community  
34 Multiscale Air Quality (CMAQ) model that agrees much better with measured dry  
35 deposition velocities across particle sizes. The key innovation is the addition of a second  
36 inertial impaction term for microscale obstacles such as leaf hairs, microscale ridges, and  
37 needleleaf edge effects. The most significant effect of the new model is to increase the  
38 mass dry deposition of the accumulation mode aerosols in CMAQ. Accumulation mode  
39 mass dry deposition velocities increase by almost an order of magnitude in forested areas  
40 with lesser increases for shorter vegetation. Peak  $PM_{2.5}$  concentrations are reduced in  
41 some forested areas by up to 40% in CMAQ simulations. Over the continuous United  
42 States, the new model reduced  $PM_{2.5}$  by an average of 16% for July 2018 at the Air  
43 Quality System monitoring sites. For summer 2018 simulations, bias and error of  $PM_{2.5}$   
44 concentrations are significantly reduced, especially in forested areas.

45 **Plain Language Summary**

46 Aerosol dry deposition is an important sink for atmospheric particles that are a health  
47 hazard and a significant climate forcer. Uncertainties in modeling aerosol dry deposition  
48 hamper accurate predictions of air quality and climate. A new aerosol dry deposition  
49 model is developed that better agrees with observations of aerosol dry deposition velocity

50 for a variety of vegetation such as forests, grasslands, and water surfaces. This improved  
51 aerosol dry deposition model when incorporated into air quality and climate models will  
52 improve the accuracy of model predictions.

53

## 54 **1. Introduction**

55 The lifetime and fate of aerosols in the atmosphere are strongly influenced by wet and  
56 dry deposition processes. Thus, the representation of these processes are key elements of  
57 atmospheric models for air quality, climate, and ecosystem impacts. The uncertainties in  
58 modeling aerosol dry deposition contribute significantly to the uncertainties and errors in  
59 direct and indirect radiative forcing that have been identified as some of the most  
60 uncertain processes in global climate modeling (IPCC, 2021). Currently, there are a wide  
61 variety of aerosol dry deposition models used in atmospheric modeling systems that  
62 reflect a great degree of uncertainty. Recently, there have been several studies that  
63 compiled observations of aerosol dry deposition in a variety of environments for particle  
64 sizes that range from 10s of nanometers to 10s of microns (Saylor et al., 2019; Emerson  
65 et al., 2020; Farmer et al., 2021). Saylor et al. (2019) showed that models differ greatly  
66 from the observations especially for forested landscapes. In some size ranges the models  
67 predict greater deposition velocities than the observations while in other size ranges, they  
68 predict lower deposition velocities up to more than an order of magnitude.

69

70 Most aerosol dry deposition models used in large-scale air quality and climate models are  
71 combinations of mathematical algorithms representing the major processes involved in  
72 aerosol deposition as presented by Slinn (1982). All these processes have strong

73 dependencies on particle size and their combination yields a relationship with the dry  
74 deposition velocity as a function of particle diameter (i.e.,  $V_d(d_p)$ ). However, since the  
75 models in use today have been shown to not agree well with consensus of observations,  
76 particularly for forests, these models need to be re-examined and revised. Key questions  
77 include: Can the parameterizations of the major processes be revised to improve results  
78 or are there key processes that have been neglected?

79

80 The focus of this paper is to address uncertainties in the current aerosol dry deposition  
81 modeling and to propose a new model that builds on current forms but includes a key  
82 new process that greatly improves agreement with the consensus of observations.

83 Section 2 describes physical processes controlling dry deposition modeling. The  
84 proposed new model is described in Section 3. Evaluation of the new model against  
85 measurements and discussion are presented in Section 4. Section 5 presents the  
86 implementation and evaluation of the new model in the Community Multiscale Air  
87 Quality (CMAQ) model (Byun and Schere, 2006) for regional applications. Concluding  
88 remarks and future work are given in Section 6.

89

## 90 **2. Physical processes in modeling dry deposition**

91 The concept of dry deposition velocity ( $V_d$ ) is that surface flux ( $F$ ) of a trace atmospheric  
92 constituent is directly proportional to its concentration ( $C$ ) just above the surface as:

$$93 \quad F = V_d \times C \quad (1)$$

94

95 In this way physical and dynamical processes can be isolated from chemical processes.

96 The principal processes involved in aerosol dry deposition include gravitational settling,

97 Brownian diffusion, surface impaction, surface interception, and rebound. All these  
 98 processes are functions of particle diameter ( $d_p$ ) and become more effective as particle  
 99 size increases except Brownian diffusion which is most effective for ultrafine particles.  
 100 Aerosol particles are transported from the air to the surface simultaneously by turbulent  
 101 fluxes and gravitational settling. The gravitational settling velocity ( $V_g$ ) results from a  
 102 balance of gravitational and viscous drag forces as (Stokes, 1851):

$$103 \quad V_g = \frac{g\rho_p d_p^2 C_c}{18\mu} \quad (2)$$

104  
 105 where  $g$  is the gravitational acceleration,  $\rho_p$  is the particle density,  $\mu$  is the dynamic  
 106 viscosity of air and  $C_c$  is the Cunningham slip correction factor for small particles  
 107 (Cunningham, 1910). The turbulent fluxes are modeled similarly to gas dry deposition  
 108 fluxes as combinations of resistances. Flux through the turbulent surface layer is  
 109 represented by aerodynamic resistance  $R_a$  which is the same for gases and aerosols  
 110 (Pleim and Ran, 2011). However, since the no-slip condition for viscous fluids requires  
 111 that the velocity is exactly zero at the boundary, there is a very thin quasi-laminar  
 112 sublayer adjacent to all surfaces. For gases, molecular diffusion across this layer is so  
 113 efficient that the resistance presented by this layer  $R_b$  is rarely the limiting factor relative  
 114 to  $R_a$  and surface resistances. For aerosol, however,  $R_b$  is usually the most limiting  
 115 resistance because diffusion of particles (Brownian diffusion) is much slower than  
 116 molecular diffusion. Gravitational settling and turbulent fluxes are combined to compute  
 117 aerosol deposition velocity as (Venkatram and Pleim, 1999),

$$118 \quad V_d = \frac{V_g}{1 - \exp(-V_g(R_a + R_b))} \quad (3)$$

119 The quasi-laminar boundary layer resistance can be expressed in terms of collection  
 120 efficiencies  $E$  (Slinn, 1982),

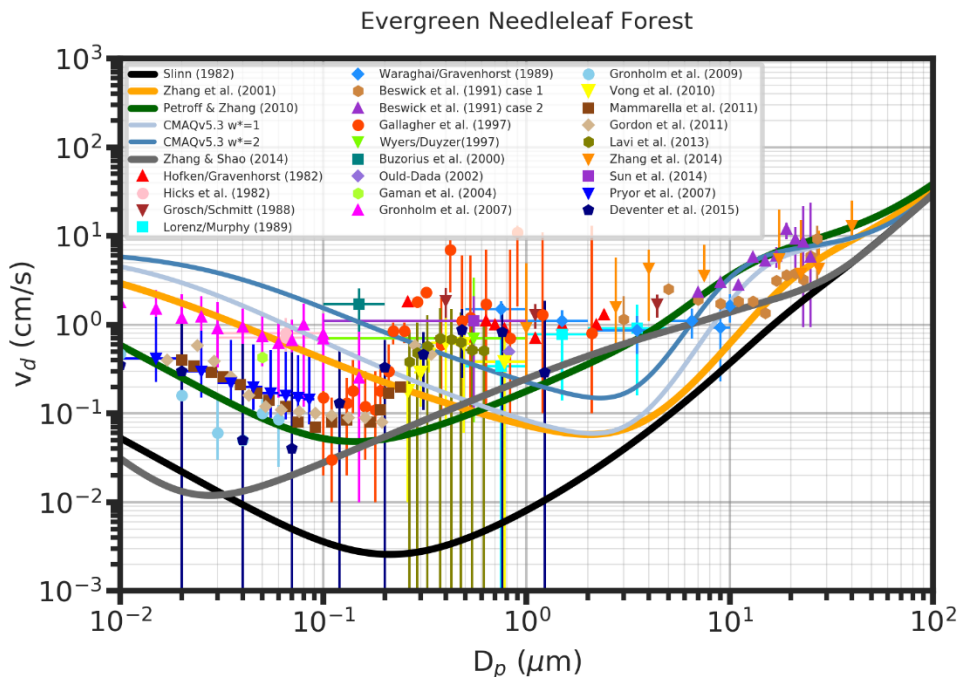
$$121 \quad R_b = \frac{1}{LAI \cdot u_* (E_B + E_{im} + E_{in}) R} \quad (4)$$

122 where  $LAI$  is leaf area index,  $u_*$  is the friction velocity,  $E_B$  is Brownian diffusion  
 123 collection efficiency,  $E_{im}$  is impaction collection efficiency, and  $E_{in}$  is interception  
 124 collection efficiency. Particles that encounter a surface can either stick or bounce off  
 125 which is represented by the rebound factor  $R$  in Equation 4 that mostly affects the largest  
 126 particles. Most recent aerosol dry deposition models follow the formulations for the  
 127 collection efficiencies proposed by Slinn (1982) with a variety of modifications and  
 128 extensions.

129

130 Aerosol deposition to vegetated areas is particularly complex and difficult to model given  
 131 the wide array of vegetation types with different canopy morphologies and leaf shapes.  
 132 Figure 1 shows that several models, including the models currently used in CMAQ, the  
 133 Comprehensive Air quality Model with extensions (CAMx) (ENVIRON, 2020), the  
 134 Goddard Earth Observing System model with Chemistry (GEOS-Chem) (Bey et al.,  
 135 2001), a Unified Regional Air-quality Modeling System (AURAMS) (Gong et al., 2006),  
 136 and the Global Environmental Multi-scale model - Modelling Air quality and CHEmistry  
 137 (GEM-MACH) (Gong et al., 2015), cannot well represent aerosol deposition for all  
 138 particle sizes at evergreen needleleaf forest sites. The current CMAQv5.3 model, which  
 139 is a modified version of the earlier CMAQ model described by Pleim and Ran (2011),  
 140 and the Zhang (2001) model that is used in CAMx, AURAMS, GEM-MACH and  
 141 GEOSChem both seem to have the wrong shape with minimum  $V_d$  at around 2-3  $\mu\text{m}$

142 while the measurements indicate minimum at about 0.1 – 0.2  $\mu\text{m}$ . The models of Petroff  
 143 and Zhang (2010) and Zhang and Shao (2014) have minimum values at much smaller  
 144 sizes with the Petroff and Zhang (2010) model agreeing well with the aggregate  
 145 observations in the less than 0.2  $\mu\text{m}$  size range. However, none of the models seem to  
 146 capture the rapid increase in deposition velocity seen in the observations from 0.2 to  
 147 about 0.5  $\mu\text{m}$  and the plateau from 0.5 to about 5  $\mu\text{m}$ . Clearly, the models as currently  
 148 formulated are not able to produce the S-shaped curve of the observation consensus.



149  
 150 Figure 1. Measured aerosol dry deposition velocities from literature as functions of  
 151 particle size for evergreen needleleaf forest. Symbols represent median values with error  
 152 bars that represent estimated uncertainty, usually inter-quartile range. The lines show  
 153 predictions by various models assuming  $u_* = 0.4$  m/s. Adapted from Saylor et al. (2019).  
 154

155 Several recent studies have shown that leaf surface texture and leaf shape have significant  
156 influence on aerosol dry deposition. For example, Chen et al. (2017) found that the  
157 needle-shaped leaves of conifers were more effective in general than broad leaves at  
158  $PM_{2.5}$  (particulate matter with an effective aerodynamic diameter less than  $2.5 \mu m$ )  
159 aerosol dry deposition. They also found that broad leaf species with more grooves or  
160 hairs tended to increase deposition. Several other studies involving both field  
161 measurements and wind-tunnel experiments also showed increased deposition for leaves  
162 with dense hairs, ridges, grooves or thick epicuticular wax layers (e.g., Weerakkody et al.,  
163 2017; Chiam et al., 2019; Leonard et al, 2016). Perini et al. (2017) also found enhanced  
164 fine aerosol deposition on leaves with thick cuticular waxes but less so for hairy leaves.  
165 By measuring aerosols accumulating on 22 species of trees and 25 shrubs, Sæbø et al.  
166 (2012) found that leaf properties such as hair and wax cover enhanced aerosol deposition  
167 among the broad-leaf species while needle-leaf species were also among the highest  
168 aerosol collecting species. Beckett et al. (2000) found greater deposition of  $1 \mu m$  aerosols  
169 on pine needles than broad flat leaves in wind-tunnel studies. They noted that deposition  
170 was well correlated with Stokes number which is inversely proportional to the  
171 characteristic leaf size which for needles was on the order of 1 mm and about 5 cm or  
172 more for broad leaves. Zhang et al. (2021) tested the effects of leaf hair (trichome)  
173 density, leaf aspect ratio, petiole (leaf stem) length, and leaf fractal deviation on  $PM_{2.5}$   
174 deposition. They found higher trichome density, lower aspect ratio, shorter petiole, and  
175 greater leaf fractal deviation all increase  $PM_{2.5}$  dry deposition velocities.

176

### 177 **3. New model description**

178 The new model, which is intended to replace the current aerosol dry deposition scheme in  
 179 CMAQ, follows the same general framework that was originally proposed by Slinn  
 180 (1982) as shown in equations 3 and 4. The aerodynamic resistance is unchanged from the  
 181 current CMAQ model and is the same for gases and aerosols (Pleim and Ran, 2011).  
 182 Unlike the current scheme, calculation of the quasi-laminar boundary layer resistance  $R_b$   
 183 differs for the vegetated and non-vegetated parts of each grid cell. The most important  
 184 change is to the parameterization of the impaction collection efficiency where a term is  
 185 added to better represent the shape of the deposition velocity curve for vegetated areas.

186

### 187 **3.1 Vegetated areas**

188 For the vegetated fraction of each grid cell the  $R_b$  is weighted by LAI to account for the  
 189 total leaf surface area density available for deposition as shown in Equation 4. The  
 190 Brownian collection efficiency  $E_B$  follows Slinn (1982) as:

$$191 \quad E_B = \left( \frac{c_v}{c_d} \right) Sc^{-2/3} \quad (5)$$

192 where  $Sc$  is the Schmidt number defined as the ratio of the kinematic viscosity of air  
 193 divided by the Brownian diffusivity  $Sc = \nu/D_B$  and  $c_v/c_d$  is the ratio of viscous drag to  
 194 total drag which we specify as 1/3 as deduced by Chamberlain (1966) for grass.

195 A key innovation in the new model to better fit observed dry deposition velocities by  
 196 particle size is to represent the impaction efficiency by two terms to account for the  
 197 effects of macroscale and microscale obstacles. Impaction efficiency  $E_{im}$  is generally  
 198 expressed as a function of Stokes number  $St$ , which describes the tendency of a particle to  
 199 follow fluid flow around obstacles. In the quasi-laminar sub-layer, the relevant flow  
 200 velocity is given by the turbulent friction velocity  $u_*$  which is the characteristic velocity

201 of turbulent eddies in the turbulent layer above the quasi-laminar sub-layer. Therefore,  
 202 for vegetated surfaces,  $St$  is defined as,

$$203 \quad St = \frac{V_g u_*}{gA} \quad (6)$$

204 where  $A$  is the characteristic dimension of the obstacles. For the new model, we define  
 205  $St_l$  and  $St_h$  using different obstacle characteristic dimensions for the leaf scale  $A_l$  and  
 206 microscale  $A_h$  representing features such as leaf hairs (trichomes) or other microscale  
 207 roughness on leaves. Thus,  $E_{im}$  is given as,

$$208 \quad E_{im} = (1 - f_{micro}) \frac{St_l^2}{1 + St_l^2} + f_{micro} \frac{St_h^2}{1 + St_h^2} \quad (7)$$

209 where  $f_{micro}$  is the fraction of total impaction due to the microscale features. The concept  
 210 of using macro and microscale obstacle size scales was introduced by Slinn (1982) for  
 211 interception processes. Slinn (1982) speculated that the microscale obstacles would  
 212 probably not be relevant for impaction because the vegetative hairs or other microscale  
 213 obstacles such as cobwebs would be deflected by the flow and not be significant  
 214 collectors by impaction. However, testing the two-term approach for both interception  
 215 and impaction showed that expressing impaction as in Equation 7 matched the size  
 216 dependent deposition velocities, especially for forests, much better than using a similar  
 217 expression for interception only. Note that both  $f_{micro}$  and  $A_h$  are very uncertain  
 218 parameters. Slinn (1982) suggested  $f_{micro} = 1\%$  but we found better fit to observations  
 219 with a slight reduction to  $f_{micro} = 0.8\%$ . The microscale characteristic obstacle scale is  
 220 specified by land use category (LUC) such that  $A_h = 0.5 \mu\text{m}$  for needleleaf forest and  
 221 grasslands and  $A_h = 1.0 \mu\text{m}$  for deciduous forest. The macroscale characteristic obstacle  
 222 scale is also specified by LUC with values ranging from 0.5 to 10 mm (Table 1).

223

224 The third collection efficiency in Equation 4 is interception. Interception is postulated as  
 225 capture that occurs when a particle comes within a particle radius of a surface or obstacle.  
 226 However, the physical basis of this process is less well defined than the Brownian or  
 227 impaction processes. Including interception efficiency as recommended by Slinn (1982)  
 228 had very little effect in the new model. Therefore, in the new model the interception  
 229 collection efficiency is not used.

230 Table 1. Key parameters for new aerosol dry deposition model over different landscapes

LU Type	$U_*$ (m/s)	LAI	$f_v$	$f_{\text{micro}}$	$A_l$ (mm)	$A_h$ ( $\mu\text{m}$ )
Needleleaf forest	0.4	5	93	0.008	2	0.5
Broadleaf forest	0.4	5	93	0.008	10	1.0
Grassland	0.3	2	95	0.002	0.5	0.5
Water	0.2	0	0	NA	NA	NA

231

### 232 3.2 Non-vegetated areas

233 For non-vegetated areas the definition of  $E_B$  is the same as for vegetated areas but the  $E_{im}$   
 234 is different,

$$235 \quad E_{im} = 10^{-3/St} \quad (8)$$

236 where,

$$237 \quad St = \frac{\rho_a V_g u_*^2}{g\mu} \quad (9)$$

238 These are the formulations recommended by Slinn (1977) for smooth surfaces where  $\rho_a$   
 239 is the air density. For water surfaces, the effects of whitecaps (breaking waves) are  
 240 included in an additional term in the  $E_B$  expression,

$$241 \quad E_B = (1 - f_{wc}) \left( \frac{C_v}{C_d} \right) S C^{-2/3} + f_{wc} \frac{u_*}{U_{10}} \quad (10)$$

242 as suggested by Pryor (1999) following Hummelshøj et al. (1992) where  $U_{10}$  is the  
 243 windspeed at 10 m above the surface. Note that the more complex form in Pryor (1999)  
 244 was not used because the term describing the particle capture by spray droplets is always  
 245 much smaller than the  $u_*/U_{10}$  term. The effects of whitecaps increase rapidly with  
 246 increasing windspeed as whitecaps cover more of the water surface. While most models  
 247 parameterize the whitecap surface fraction  $f_{wc}$  as a function of windspeed, we follow  
 248 Albert et al. (2016) who developed a parameterization based on satellite whitecap  
 249 fraction data, that is also a function of water surface temperature  $T_{ws}$  in Celsius and  $U_{10}$  is  
 250 in m/s,

$$251 \quad f_{wc} = a(b + U_{10})^2 \quad (11)$$

$$252 \quad \text{where} \quad a = a_1 + a_2 T_{ws} + a_3 T_{ws}^2$$

$$253 \quad b = b_1 + b_2 T_{ws}$$

254 and  $a_1 = 8.46 \times 10^{-5}$ ,  $a_2 = 1.63 \times 10^{-6}$ ,  $a_3 = -3.35 \times 10^{-8}$ ,  $b_1 = 3.354$ , and  $b_2 = -0.062$ .

255

256 Another new modification is for the non-vegetated parts of urban LU categories where  $R_b$   
 257 is weighted by building area index ( $BAI$ ). The rationale for this is that buildings add  
 258 significant surface area in urban landscapes that is not accounted for by LAI or otherwise.

259 An initial estimate is  $BAI = (4 \lambda_f + 1)/(1 - f_v)$ , where  $\lambda_f$  is frontal area density of building

260 surfaces and  $f_v$  is the vegetated fraction of the grid cell. The logic for this is that the total

261 building surface area is four times the frontal area. For applications where detailed  
262 building data is not included, default values of  $BAI$  are specified by landuse category.  
263 For example,  $BAI$  is specified as 1.8, 2.0, and 2.3 for the National Land Cover Database  
264 (NLCD) categories of low intensity developed, medium intensity developed, and high  
265 intensity developed, respectfully. For all other non-developed categories,  $BAI$  is set to 1.  
266 Thus, for unvegetated portions of urban grid cells  $R_b$  is defined as,

$$267 \quad R_b = \frac{1}{BAI \cdot u_* (E_b + E_{im})} \quad (12)$$

268 Note that particle rebound effects are not considered ( $R=1$ ) because only the largest  
269 particles are affected and there is much variation by composition, RH, surface type, and  
270 windspeed. Grid cell deposition velocity is the combination of the vegetated and non-  
271 vegetated parts,

$$272 \quad V_d = f_v V_{dveg} + (1 - f_v) V_{dnoveg} \quad (13)$$

273

274

## 275 **4. New model evaluation**

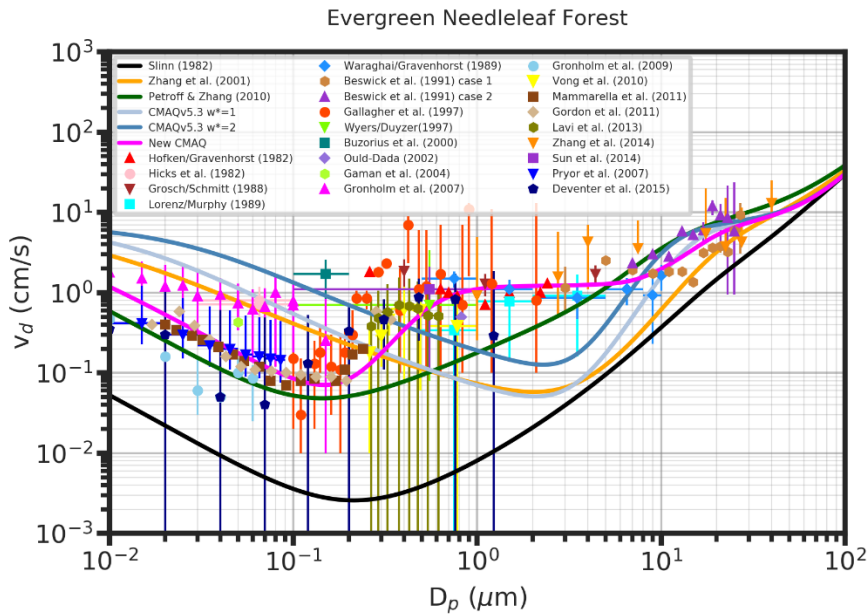
276 The new model is evaluated against aerosol dry deposition measurements over different  
277 landscapes. The performance of the new approach is also discussed in terms of the  
278 enhanced processes.

279

### 280 **4.1 Comparison to measurements**

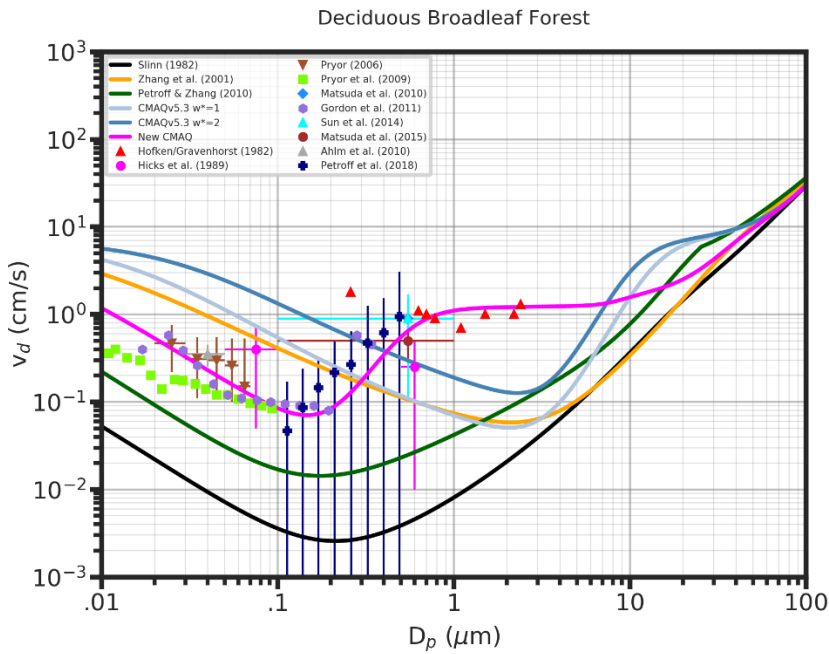
281 Following several recent papers (Saylor et al., 2019; Emerson et al., 2020; Farmer et al.,  
282 2021), we compile aerosol dry deposition measurements by particle size for various  
283 surface types from the published literature to compare to aerosol dry deposition models.

284 Figure 2 shows the same data for evergreen needleleaf forest as figure 1 with the addition  
 285 of the new model described here. The parameter values for the model runs for each land  
 286 use type are shown in Table 1. Note that the new model, designated *New CMAQ*, is the  
 287 only one that shows the increase of  $V_d$  in the  $0.2 - 0.6 \mu\text{m}$  range and the plateau from  
 288 about  $0.6 \mu\text{m}$  to  $6 \mu\text{m}$ . It is also the only model that does not substantially underpredict  
 289  $V_d$  from  $0.2 - 3.0 \mu\text{m}$ . This has profound effects on dry deposition and concentration of  
 290  $\text{PM}_{2.5}$  as will be shown in Section 5.  
 291

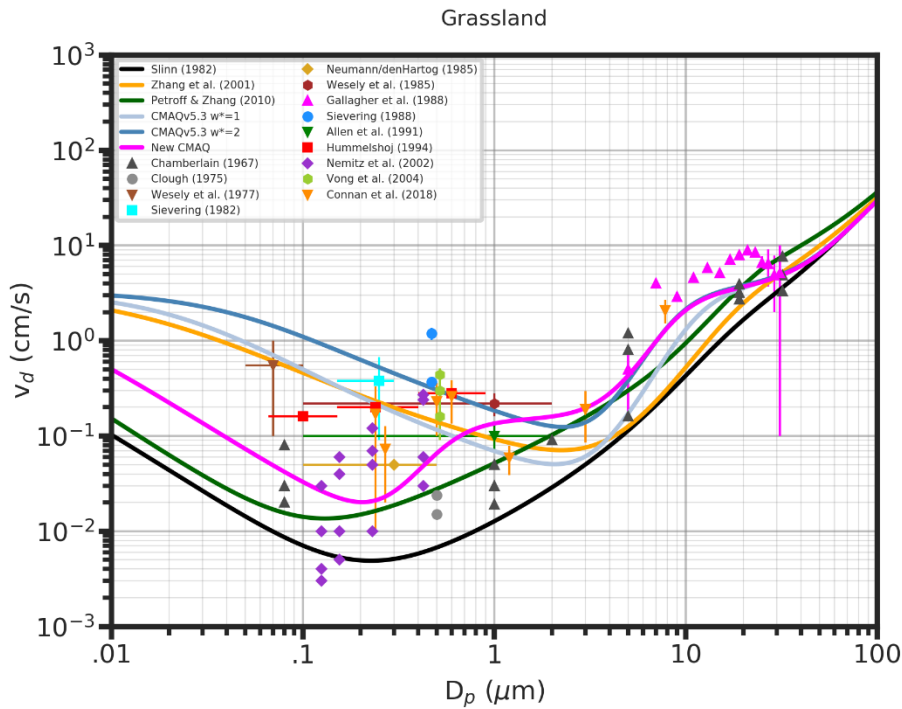


292  
 293 Figure 2. Same as Figure 1 but with the addition of the new model.  
 294  
 295 There are not as many measurement studies in the literature for other landuse/vegetation  
 296 types. Figure 3 shows the observation data and models for deciduous broadleaf forest.  
 297 The consensus of dry deposition measurements to broadleaf forests suggests a similar

298 shape to the  $V_d$  vs  $d_p$  curve where there is an increase of  $V_d$  in the approximately 0.2 to  
 299 0.6  $\mu\text{m}$  range with a plateau up to about 6  $\mu\text{m}$ . Again, the new model is the only one that  
 300 replicates the shape of this curve and does not greatly underestimate  $V_d$  in the 0.5 - 4.0  
 301  $\mu\text{m}$  range.  
 302



303  
 304 Figure 3. Same as figure 2 but for deciduous broadleaf forest.



305

306

307

308 Figure 4. Same as figure 2 but for grasslands.

309

310 Figure 4 shows the new model and other models for grasslands compared to  
 311 measurements. While there are a lot of measurements for grasslands, there seems to be  
 312 much less consensus among them, even within the same studies, than for forests. With  
 313 the degree of scatter in the measurements there isn't clear guidance for parameter  
 314 selection. While the rationale for microscale impaction may also apply to grass since  
 315 grass leaves often have leaf hairs or trichomes and serrated edges, the evidence from the  
 316 measurements is less clear. Therefore, the parameter values selected for the microscale  
 317 impaction scaling factor  $f_{micro}$  are set to smaller values (see Table 1) than for forests,  
 318 which seem to better fit with the measurements. Running box models on an hourly or

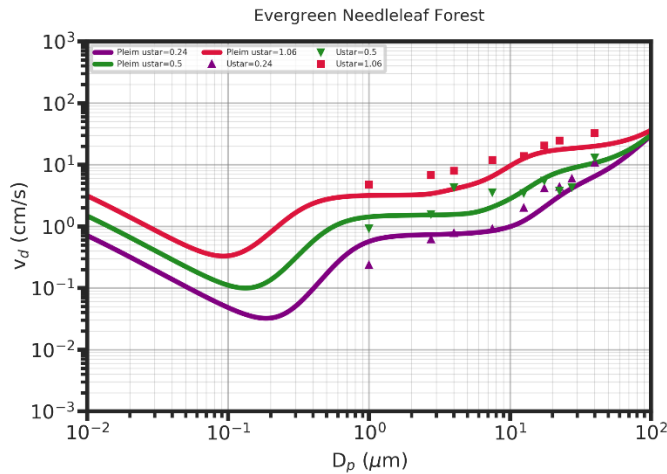
319 sub-hourly basis using detailed field measurements may add some clarity to model  
320 performance and refinement of parameters.

321

322 The large scatter among the reported measurements for grassland is likely due the variety  
323 of grass species which can have very different characteristics including length. For  
324 example, the measurements reported by Vong et al. (2004) were made over rye grass 0.75  
325 - 1 m tall, Allen et al. (1991) measured deposition to short grass of 3 – 7 cm in length,  
326 Conan et al. (2018) used artificial grass, and Nemitz et al. (2002) measured in a moorland  
327 which is characterized by hummocks and hollows with vegetation including peat moss  
328 (*Sphagnum*) and several species of tall grasses.

329

330 Virtually all studies found strong dependences of  $V_d$  on  $u_*$  with  $V_d$  increasing with  
331 increasing  $u_*$  (Pryor et al., 2008). Some have suggested that  $V_d/u_*$  is a more robust  
332 quantity for analysis and comparison (e.g., Conan et al., 2018) but many studies did not  
333 report this. Zhang et al. (2014) measured dry deposition velocities of dust particles (1 –  
334 40  $\mu\text{m}$ ) in a wind tunnel at various wind velocities over different surfaces. To simulate  
335 deposition to trees, evergreen branches were planted in the test section surface. The new  
336 model set up for evergreen needleleaf forest is shown (Figure 5) to compare well to the  
337 tree wind tunnel experiments at three windspeeds with measured friction velocities of  
338 0.24, 0.5, and 1.06 m/s.



339

340 Figure 5. New model compared to wind tunnel experiments for tree surfaces (Zhang et  
 341 al. 2014) at three friction velocities.

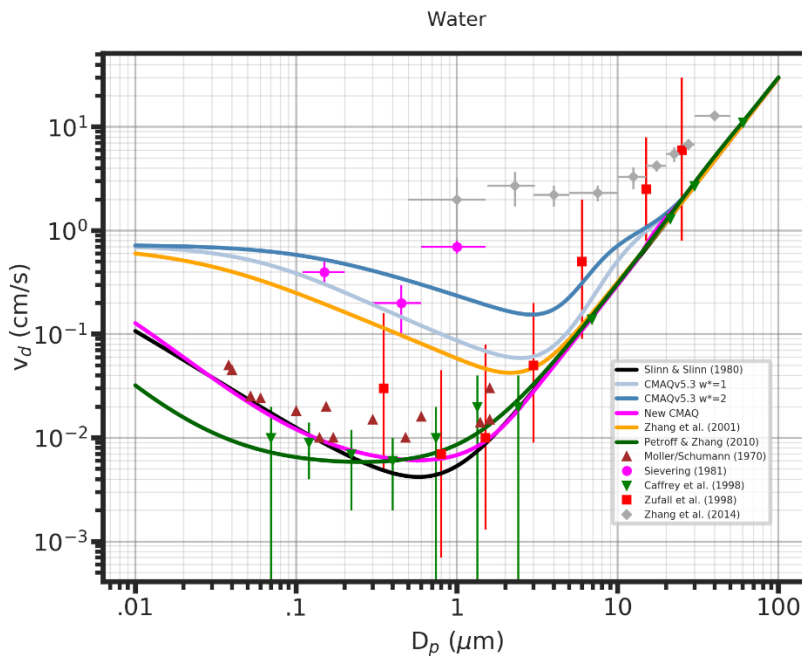
342

343 Figure 6 shows models compared to field measurements for water surfaces. Most of the  
 344 measurements over water show that dry deposition velocities are much lower in the  
 345 accumulation size range than for vegetated surfaces. The measurements by Sievering  
 346 (1981) seem to be outliers with much higher deposition velocities in the 0.15 – 1  $\mu\text{m}$   
 347 range. These measurements, which used the momentum gradient technique that assumes  
 348 similarity between aerosol fluxes and momentum fluxes, can be particularly uncertain  
 349 when the surface has bluff bodies such as waves than can induce form drag on  
 350 momentum flux. The other outlier study is by Zhang et al. (2014) which is a wind tunnel  
 351 study where dry deposition velocity is estimated by particle dynamic analysis (PDA).  
 352 The measurements over water in the wind tunnel were found to agree quite well with the  
 353 Slinn and Slinn (1980) (SS80) model for three different friction velocities when  $R_b$  is set  
 354 to zero (Zhang et al., 2014, Figure 11). The authors hypothesize that this is due to waves

355 and spray droplets. However, given the dramatic dissimilarity from most of the other  
 356 studies, there could be an issue of scaling wave-wind dynamics to a wind tunnel where  
 357 the water is very shallow with restricted fetch.

358

359 The new model agrees well with the measurements other than the 2 outlier studies and is  
 360 most similar to the SS80 model. The main difference in formulation between the new  
 361 model and the SS80 model for water is the inclusion of the effects of whitecaps in  
 362 enhancing deposition velocity. Since Equation 11 does not have any dependence on  $d_p$   
 363 the whitecaps effects are effectively a lower limit on  $V_d$  which raises the trough of the  
 364 curve.



365

366 Figure 6. Same as Figure 2 but for water surfaces.

367

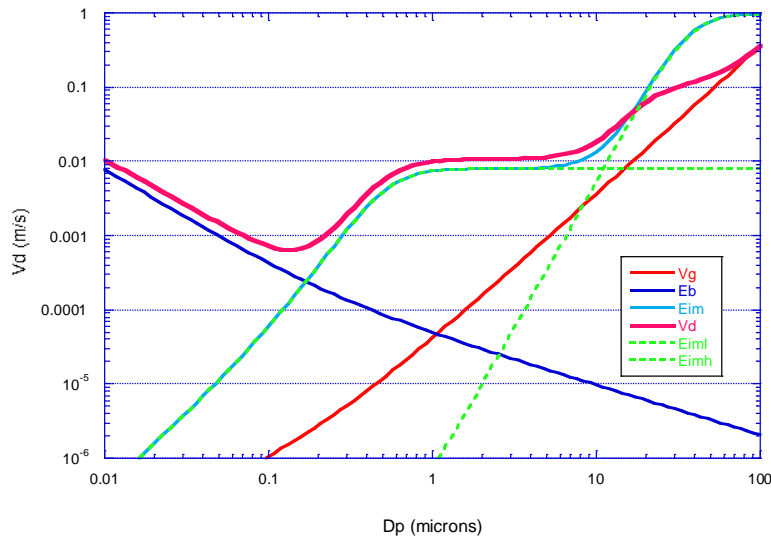
368 **4.2 Discussion**

369 Figure 7 shows the size dependence of the components of the dry deposition model for  
370 needleleaf forest. Clearly, the most effective component responsible for the S-shape  
371 curve for vegetated surfaces in the 0.2 – 10  $\mu\text{m}$  range is the impaction on microscale  
372 features. The impaction collection efficiency acts as a threshold process where  $E = 1$   
373 where  $St > \sim 3$  for the formulation shown in Equation 7 and ramps down as  $St$  and  $d_p$  get  
374 smaller. The Stokes number, as represented by Equation 6, is a ratio of the inertial  
375 stopping distance of a particle to a characteristic length scale of an obstacle. For the  
376 macroscale term, which is common to nearly all current aerosol deposition models, the  
377 characteristic length represents the effects of the leaves. Figure 7 shows that the leaf  
378 scale impaction term has greatest effect on particles larger than about 5  $\mu\text{m}$ . Note that for  
379 broadleaf forests the effects of this term are limited to even larger particles because the  
380 characteristic length scale is greater for broad leaves than for needle leaves.

381

382 The stopping distance for quasi-laminar sublayers on leaves can be estimated as  $V_g u^*/g$ .  
383 For  $u^* = 0.4$  m/s the stopping distance decreases with decreasing  $d_p$  reaching 1  $\mu\text{m}$  at  $d_p =$   
384 0.75  $\mu\text{m}$ . A characteristic length of about 0.5  $\mu\text{m}$  and a scaling factor  $f_{micro}$  of about  
385 0.008 result in a good fit to the measured data as shown in Figure 2. A physical  
386 explanation of this process is that there exist microscale features on many leaves and  
387 stems that act as obstacles in the quasi-laminar sublayers. Many studies have shown  
388 increased deposition of  $\text{PM}_{2.5}$  for broadleaf species that have dense hairs, ridges, grooves,  
389 or thick epicuticular wax layers as summarized above in Section 2. While needleleaf  
390 species generally don't have leaf hairs, they are often seen to be particularly efficient at  
391  $\text{PM}_{2.5}$  collection. A possible explanation is the narrow needle shape of the leaves may

392 cause the sublayers to thin toward the edges of the leaves. Since the needle shape  
 393 presents far more edge to the flow per area than broad leaves the deposition of sub-  
 394 micron sized particles is more efficient. The hypothesis that more edge per area increases  
 395 deposition is supported by the results of Zhang et al (2021) that showed increased  $PM_{2.5}$   
 396 deposition to leaves with lower aspect ratio and greater fractal deviation. A physical  
 397 interpretation of the scaling factor is that the edge effects of needle shaped leaves is only  
 398 affecting a small portion of the leaf area. For broadleaf forest, the scaling factor accounts  
 399 for the fraction of species that have dense leaf hairs or other microscale features and the  
 400 sparsity of these features per leaf area.



401  
 402 Figure 7. Size dependence of the components of the dry deposition model for needleleaf  
 403 forest.

404

### 405 **5. CMAQ implementation and evaluation**

406 The new aerosol dry deposition model is implemented in the latest version of the CMAQ  
 407 modeling system. The coupled version of the Weather Research and Forecasting

408 (WRFv4.0.2) model and the CMAQv5.3 model are used to evaluate the new approach in  
 409 air quality simulations over different-resolution domains for summer conditions in 2018.

410

### 411 **5.1 Model implementation**

412 Since CMAQ uses log-normal size distributions to represent Aitken, accumulation, and  
 413 coarse modes, aerosol deposition velocities need to be integrated over the log-normal size  
 414 distributions to calculate the 0<sup>th</sup>, 2<sup>nd</sup>, and 3<sup>rd</sup> moments which represent the number,  
 415 surface area, and volume of each mode, respectively. Therefore, the terms in the model  
 416 that have explicit dependence on particle diameter  $D$  are integrated following Binkowski  
 417 and Shankar (1995)

$$418 \quad \hat{X}_k = \frac{1}{M_k} \int_{-\infty}^{\infty} X D^k (\ln D) d \ln D \quad \text{where } M_k = N D_g^k \exp\left(\frac{k^2}{2} \ln^2 \sigma_g\right) \quad (14)$$

419 where  $k$  is the moment (0,2,3) and  $N$  is the particle number concentration. The only  
 420 terms in the new model that are explicit functions of particle diameter are Brownian  
 421 diffusivity and gravitational settling velocity. For Brownian diffusivity the integrated  
 422 form is,

$$423 \quad \hat{D}_{Bk} = D_B(D_g) \left\{ \exp\left(\frac{(-2k+1)}{2} \ln^2 \sigma_g\right) + 1.246 Kn_g \exp\left(\frac{(-4k+4)}{2} \ln^2 \sigma_g\right) \right\} \quad (15)$$

424 For gravitational settling velocity the integrated form is:

$$425 \quad \hat{V}_{gk} = V_g(D_g) \left\{ \exp\left(\frac{(4k+4)}{2} \ln^2 \sigma_g\right) + 1.246 Kn_g \exp\left(\frac{(2k+1)}{2} \ln^2 \sigma_g\right) \right\} \quad (16)$$

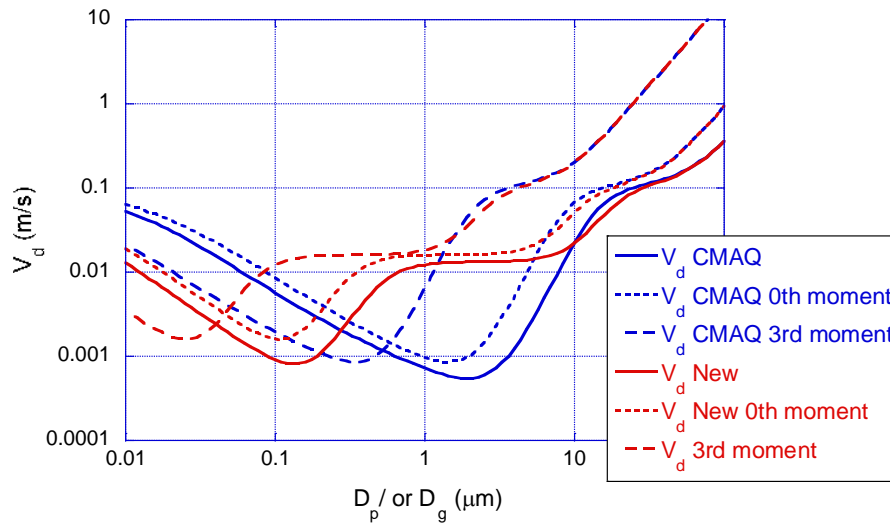
426 where  $D_g$  is the geometric mean diameter,  $\sigma_g$  is the geometric standard deviation, and the  
 427 Knudsen number is  $Kn_g = 2\lambda/D_g$  where  $\lambda$  is the mean free path. For the modal model, the  
 428 dry deposition velocity is computed as described in Section 3 but with  $\hat{D}_{Bk}$  and  $\hat{V}_{gk}$  for  $k$   
 429  $= 0,2,3$  for the three moments of each of the three modes replacing  $D_B$  and  $V_g$ .

430

431 Figure 8 demonstrates the relationships among the dry deposition velocity moments for  
432 both the CMAQv5.3 model and the new model plotted against geometric mean diameter  
433  $D_g$  compared to the non-integrated models vs particle diameter  $D_p$  applied for needleleaf  
434 forest. The 0<sup>th</sup> moment, which represents the number of the modal distribution, shows  
435 the effects of integration are to increase the  $\hat{V}_d$  over the  $V_d$  for all sizes except in the  
436 plateau range ( $\sim 1 - 3 \mu\text{m}$ ) of the new model. The 3<sup>rd</sup> moment is similar to the 0<sup>th</sup> moment  
437 but with a shift to smaller  $D_g$  because the larger end of the distribution contributes more  
438 to volume than number.

439 Since the 3<sup>rd</sup> moment is proportional to mass, the 3<sup>rd</sup> moment of the dry deposition  
440 velocity represents the dry deposition velocity for mass concentration of aerosols. From  
441 Figure 8 it is evident that the mass deposition velocity for the new model is about an  
442 order of magnitude greater in the accumulation mode ( $D_g \sim 0.1 - 0.4 \mu\text{m}$ ) than for the  
443 CMAQv5.3 model in forested areas. The effects of this increased dry deposition are  
444 assessed for CMAQ simulations across the conterminous US (CONUS) and at high  
445 resolution in the NE U.S.

446



447

448 Figure 8. The dry deposition velocities for the 0<sup>th</sup> and 3<sup>rd</sup> moments of the CMAQv5.3  
 449 model and the new model compared to the non-integrated dry deposition velocities for  
 450 both models applied to needleleaf forest. The x-axis represents  $D_g$  for the  $\hat{V}_d$  plots and  $D_p$   
 451 for the  $V_d$  plots.

452

## 453 5.2 WRF-CMAQ simulations

454 The coupled WRFv4.0.2/CMAQv5.3.1 model system was run in both the base  
 455 configuration and with the new aerosol dry deposition model for several months in  
 456 summer 2018. These simulations were based on modeling of the Long Island Sound  
 457 Tropospheric Ozone Study (LISTOS) which was an intensive multi-institutional field  
 458 study during the summer of 2018 (Karambelas 2020). The base model was run for three  
 459 resolutions (12 km, 4 km, 1.33 km) where the outer domain covered the CONUS with  
 460 one-way nested domains over the northeast (NE) states (4 km) and the New York/New  
 461 Jersey/Connecticut (NY-NJ-CT) region (1.33 km). Detailed description of the model  
 462 configuration and evaluation are presented by Torres-Vazquez et al. (2022). Model

463 simulations using the new aerosol dry deposition model (NEW) were conducted for the  
464 12 km CONUS domain for July 2018 and for the 1.33 km domain for July and August  
465 2018. In both cases, identical simulations using the base CMAQv5.3 model (BASE)  
466 were also run. Initial conditions for the 12 km CONUS runs were from base case runs on  
467 June 21, 2018, that were started on January 1, 2018. The 1.33 km runs were initialized  
468 on July 1, 2018, from base case 1.33 km runs that started on May 2, 2018. All runs used  
469 the same boundary conditions and emissions as described by Torres-Vazquez et al.  
470 (2022).

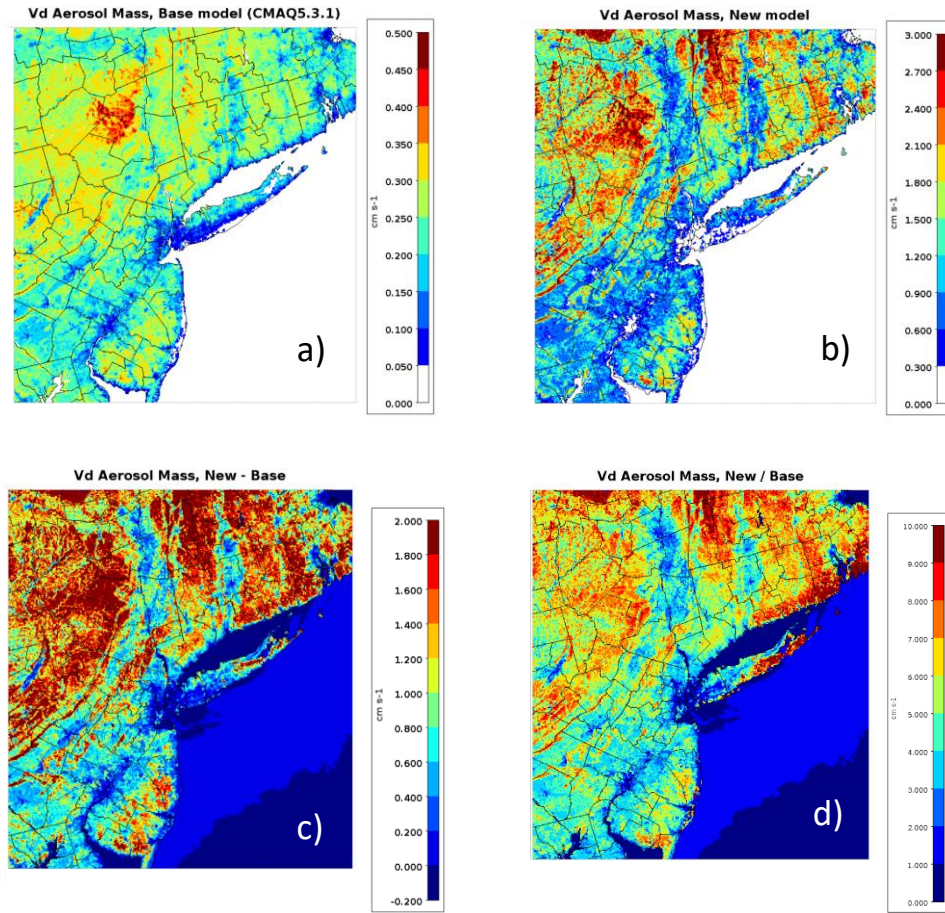
471

472

473

474

475



476

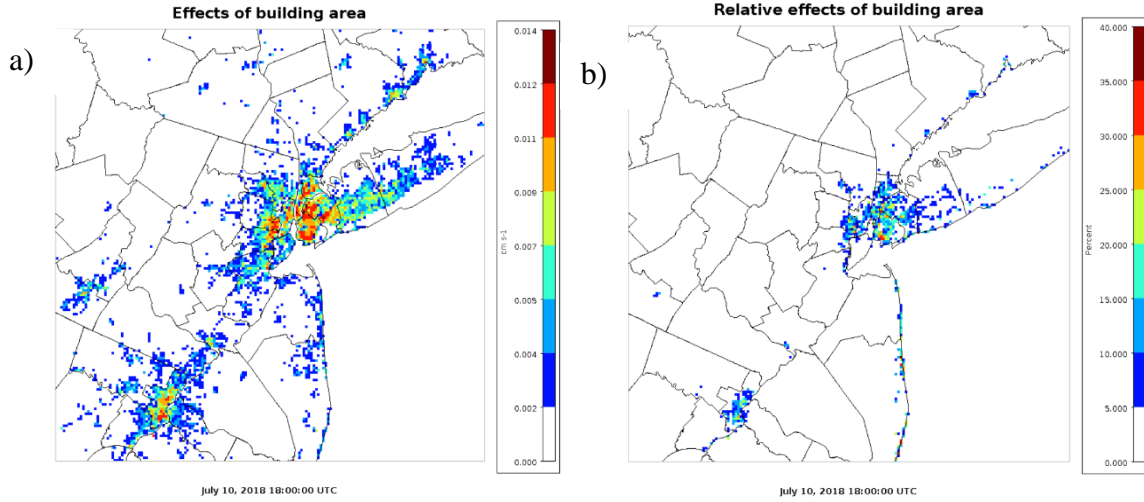
477

478 Figure 9. Accumulation mode mass dry deposition velocity from WRF-CMAQ on July  
479 10, 2018 at 18 UTC (2 pm LT) for (a) BASE, (b) NEW, (c) NEW-BASE and (d)  
480 NEW/BASE over the New York/New Jersey/Connecticut 1.33-km domain. Note that the  
481 scales for (a) and (b) are different.

482

483 Figure 9 shows the dry deposition velocity for accumulation mode mass on July 10, 2018,  
484 at 18 UTC (2 pm LT) for BASE, NEW, NEW-BASE and NEW/BASE over the NY-NJ-  
485 CT 1.33 km resolution domain. July 10 was a particularly polluted day in the NYC area.

486 Thus, it is an interesting case to study the effects of the new aerosol dry deposition  
487 model. The plots in Figure 9a and 9b both show how variations in land use strongly  
488 influence aerosol dry deposition for both BASE and NEW with greatest  $V_d$  in the forested  
489 areas. This is due to the combinations of large roughness length resulting in low  
490 aerodynamic resistance and large LAI. The greatest effects of the new model are  
491 indicated by the difference in the plot scales (BASE plots 0-0.5 cm/s; NEW plots 0-3.0  
492 cm/s) which reflects an almost order of magnitude increase in  $V_d$  for accumulation mode  
493 mass in forested areas. Figures 9c and 9d, NEW – BASE and NEW/BASE, respectively,  
494 demonstrate that the largest differences are in the forested areas of Pennsylvania (PA),  
495 NY, Massachusetts (MA), CT, and Rhode Island (RI). The ratio of NEW/BASE (Figure  
496 9d) is a factor of 8-10 in the heavily forested areas while it is only 1-3 in developed areas  
497 depending on the intensity of development. The inclusion of the building area as in  
498 Equation 12 increases  $V_d$  for accumulation mode mass in developed areas but only by a  
499 small amount as shown in Figure 10a. However, because the  $V_d$  in developed areas is  
500 small compared to vegetated areas, inclusion of the building effects has a substantial  
501 relative impact on the  $V_d$  (Figure 10b).



502

503

504

505

506

507

508

509

510

511

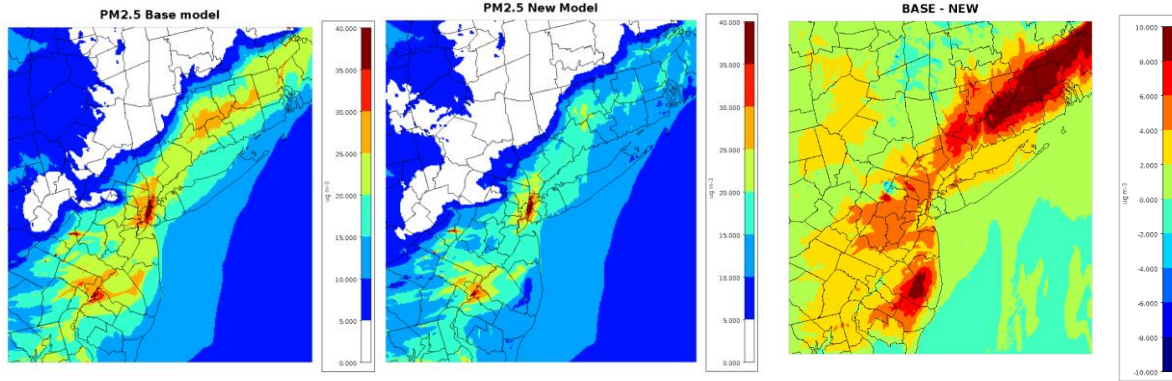
512 Figure 10. Difference (a) and relative difference (b) in  $V_d$  for accumulation mode mass

513 between a NEW model run using  $BAI$  as in Equation 12 and a NEW mode run where  $BAI$

514 = 1 for July 10, 2018, at 18 UTC over the New York/New Jersey/Connecticut 1.33-km

515 domain.

516



517

518 Figure 11. PM<sub>2.5</sub> concentration on July 11, 2018, at 00 UTC (July 10, 8 pm LT) for  
 519 BASE model (a) NEW model (b), and BASE - NEW (c) over the 1.33 km resolution  
 520 domain.

521

522 Figure 11 shows the consequences of the new aerosol deposition velocities, shown in  
 523 Figure 9, on PM<sub>2.5</sub> concentrations 6 hours later when the highest concentrations occurred  
 524 in the region. The PM<sub>2.5</sub> concentrations at this time are greatest in the urban centers of  
 525 NY city (NYC) and Philadelphia with high concentrations downwind to the northeast into  
 526 CT and RI. The biggest effect of the new aerosol dry deposition is to substantially reduce  
 527 the downwind concentrations in southern New England which is mostly forested.

528 Another relative concentration maximum in the BASE model in southeastern NJ in an  
 529 area known as the Pine Barrens, which is dense forest with a high fraction of needleleaf  
 530 trees, is mostly absent in the NEW model run. Thus, the NEW model has larger effects  
 531 on PM<sub>2.5</sub> concentrations in forested areas than other areas such as in urban areas. The  
 532 peak concentrations in NYC only reduced by 10% while in some of the forested areas the  
 533 NEW simulation reduces PM<sub>2.5</sub> concentration by more than 40%.

534

535 The afternoon (18 – 20 UTC) deposition velocity for accumulation mode mass was  
 536 averaged for July 2018 for BASE and NEW model runs for the CONUS at 12 km  
 537 resolution (Figure 12). Again, it is evident that the largest effects of the NEW model are  
 538 in the forested areas mostly in the NE, western mountains and across the boreal forests of  
 539 Canada. In some areas of the northeastern U.S. and southeastern Canada the NEW dry  
 540 deposition velocities are 7-10 times the BASE values (Figure 12d). Note that Figure 12a  
 541 shows some discontinuities at the Canadian border. This is due to the hybrid land use  
 542 data that is a combination of higher resolution NLCD for the CONUS and the lower  
 543 resolution Moderate Resolution Imaging Spectroradiometer (MODIS) land use data for  
 544 elsewhere (Torres-Vazquez et al., 2022; Appel et al. 2014). In some of the sparsely  
 545 vegetated areas in the west the difference between NEW and BASE is quite small while  
 546 in the plains and predominately agricultural areas the difference is moderate.

547

548

549

550

551

552

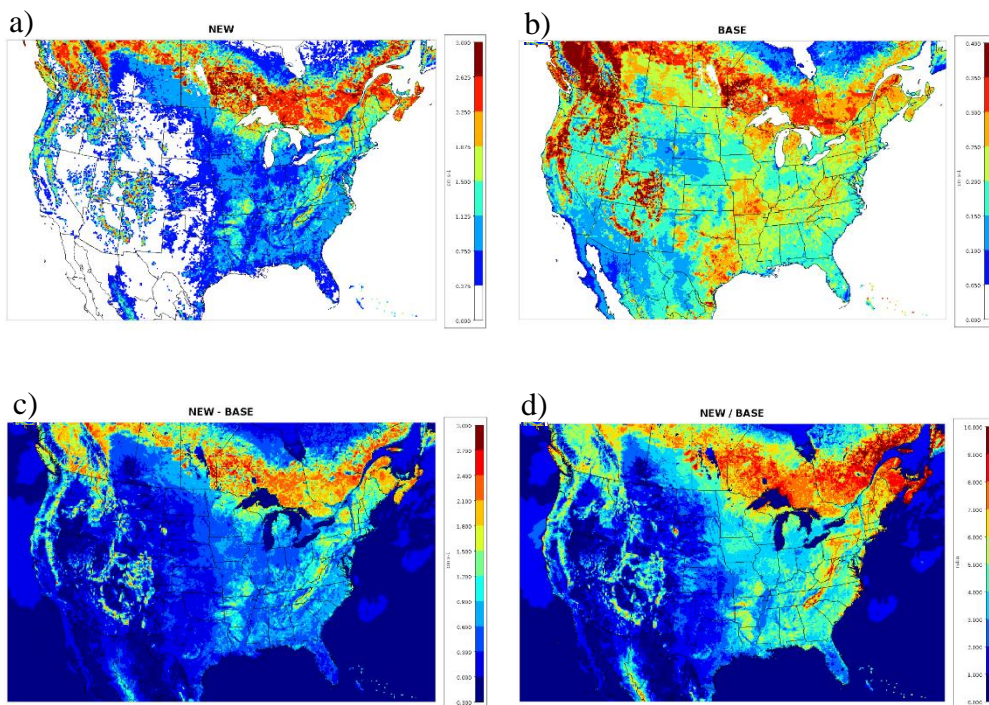
553

554

555

556

557



558

559

560

c)

d)

561

Figure 12. Afternoon (18 – 20 UTC) average accumulation mode mass dry deposition

562

velocity for July 2018 on the CONUS 12 km domain for (a) BASE, (b) NEW, (c) NEW-

563

BASE and (d) NEW/BASE. Note that the scales for (a) and (b) are different.

564

565

Increases in dry deposition velocity for accumulation mode aerosol using the NEW

566

model increase the loading of aerosol species to land ecosystems. For example, Figure

567

13 shows that accumulated dry deposition mass of accumulation plus Aitken mode

568

(approximately  $< 2.5 \mu\text{m}$ ) ammonium aerosol for July 2018 is much greater for the NEW

569

model than the BASE model. Thus, the NEW model has much greater predictions of

570

nutrient loading of the aerosol components, especially to forested ecosystems. The NEW

571

model increases deposition of other aerosol species as well that have may have health

572

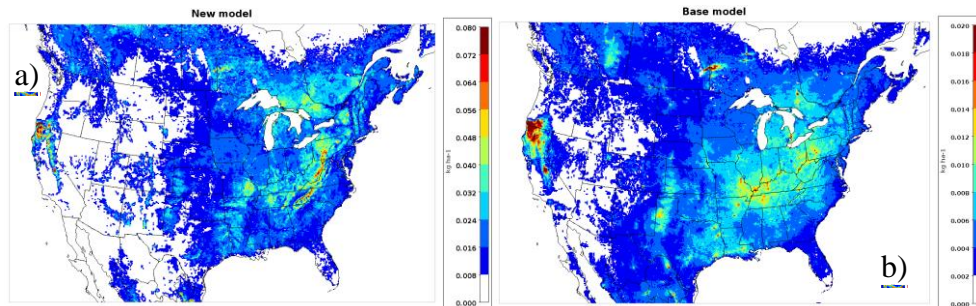
effects on livestock and wildlife. Predictions of exposure to hazardous chemicals, which

573

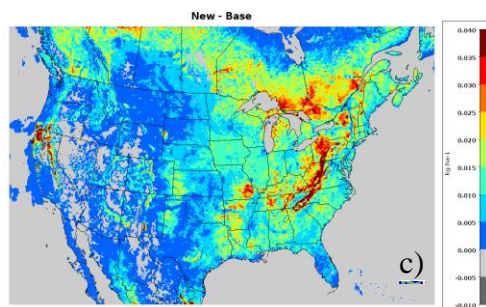
may affect human health through ingestion of soil or contaminated produce, also increase

574

with the NEW model.



575



576

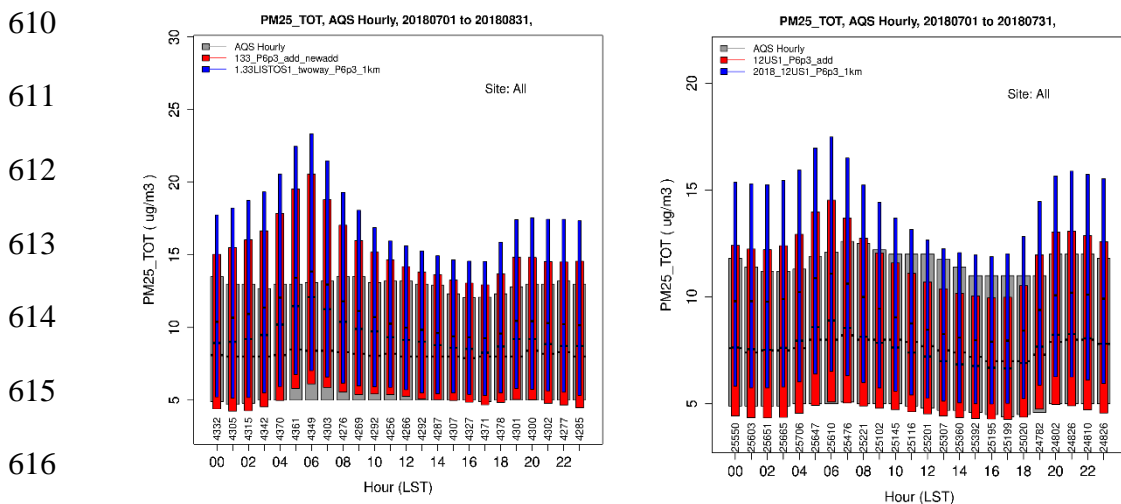
577 Figure 13. Accumulated dry deposition (kg/ha) over July 2018 of ammonium aerosol in  
 578 accumulation plus Aitken modes. NEW model (a), BASE model (b) and NEW – BASE  
 579 (c). Note that the scale for NEW model (a) is four times the scale for BASE model (b)

580

### 581 **5.3 Simulation evaluation**

582 The WRF-CMAQ simulations at both 1.33 km grid resolution in the NYC area and 12  
 583 km grid resolution for the CONUS were evaluated for PM<sub>2.5</sub> at the U.S. Environmental  
 584 Protection Agency (EPA) Air Quality System (AQS) sites. Evaluations of model runs  
 585 using the NEW aerosol dry deposition model were compared to the BASE model for  
 586 summer season when the differences between NEW and BASE are greatest. Figure 14  
 587 shows diurnal bar charts for July and August 2018 for all AQS sites in the 1.33 km grid  
 588 resolution domain (see figure 9 for size of domain) and for July 2018 at AQS sites in the  
 589 12 km grid resolution CONUS domain. The colored bars represent the 25<sup>th</sup> and 75<sup>th</sup>  
 590 percentiles of the PM<sub>2.5</sub> concentration distributions for NEW, BASE, and AQS. The  
 591 black line in each bar indicates the median value. For the fine grid NE domain both  
 592 NEW and BASE are high compared to AQS for every hour but NEW is closer to AQS.  
 593 The diurnal pattern of the modeled concentrations is different from the observation with  
 594 the greatest concentrations around 6 am and lowest in late afternoon at about 17 LT while  
 595 the AQS concentrations show very little diurnal variation. This diurnal pattern is typical

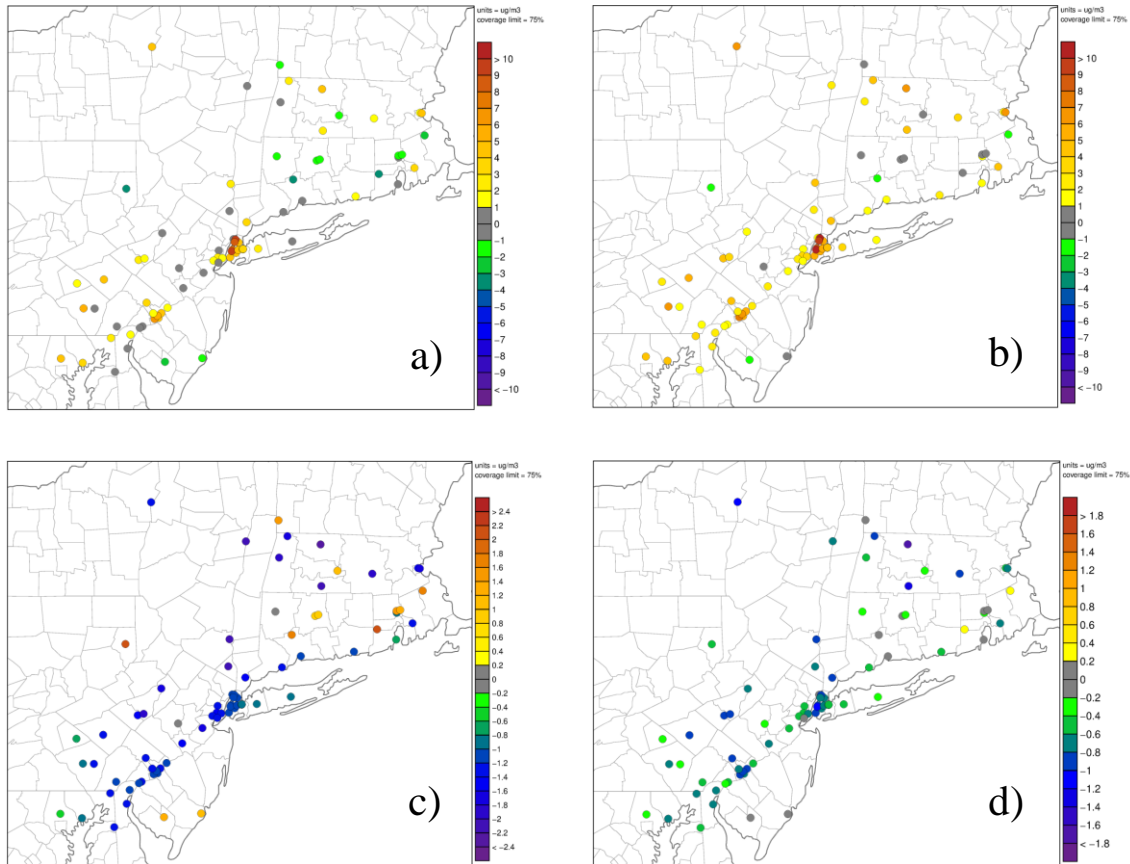
596 for modeled concentrations of species with a large ground emitted fraction (i.e., NO<sub>x</sub>,  
 597 CO, and PM<sub>2.5</sub>). This is a known issue that is related to the suppressed vertical mixing at  
 598 night and the much greater mixing during the day. The near dawn peak results from the  
 599 combination of suppressed mixing and high emissions during the morning rush hour.  
 600 Note that this issue has been improved in recent years through updates to the PBL  
 601 scheme in the WRF-CMAQ system (e.g., Toro et al., 2021). Another contributing factor  
 602 is the uncertainty in emissions and especially the hourly attribution of emissions.  
 603  
 604 Evaluation of the 12 km CONUS simulations shows similar diurnal pattern with peak  
 605 concentrations around sunrise and lowest concentrations in afternoon (EDT). The AQS  
 606 concentrations are more constant over the day than the models but with a slight variation  
 607 with a similar diurnal pattern. The BASE model is again higher than the observations for  
 608 every hour, but the NEW model is slightly high during the night and slightly low during  
 609 the day.



617 Figure 14. Hourly bar plots of PM<sub>2.5</sub> aggregated over July and August 2018 for the  
 618 northeast 1.33 km domain on left and over July 2018 for the 12 km CONUS on right. The

619 colored bars represent the 25<sup>th</sup> and 75<sup>th</sup> percentiles of the PM<sub>2.5</sub> concentration  
620 distributions for NEW (red), BASE (blue), and AQS observations (grey).  
621  
622 Spatial evaluation of PM<sub>2.5</sub> in the 1.33 km domain for NEW and BASE are shown in  
623 Figure 15. For both NEW and BASE the average bias is greatest in NYC where high  
624 emissions are concentrated in small grid cells. The BASE (15b) also has high bias at  
625 most other sites. The NEW (15a) has less high bias and is roughly even between slightly  
626 high and slightly low biases outside of NYC. The lower plots show reduced bias (15d)  
627 and mean error (15c) for NEW compared to BASE at 83% and 93% of the AQS sites,  
628 respectively. The urban effects of building area reduce the high bias in the cities but only  
629 by a very small amount (less than 0.3%; not shown).

630



631

632

633 Figure 15. Evaluation of modeled hourly PM<sub>2.5</sub> compared to AQS measurements

634 averaged for July and August 2018: (a) NEW model bias, (b) BASE model bias, (c)

635 NEW – BASE absolute bias difference, and (d) NEW – BASE mean absolute error

636 difference.

637

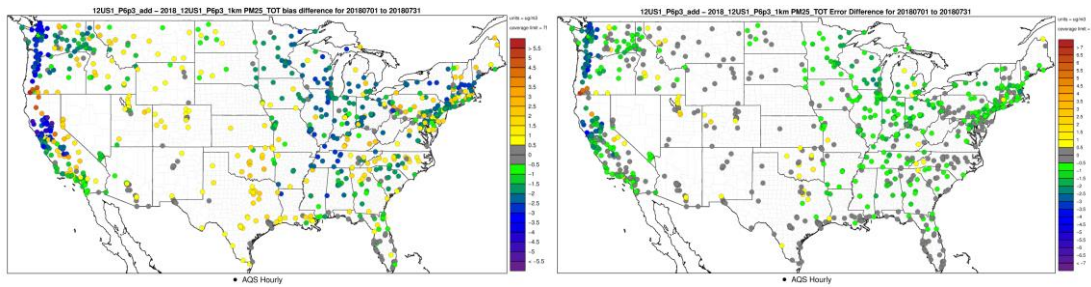
638 Similar spatial evaluation for the 12 km CONUS simulations is shown in Figure 16.

639 Overall, the PM<sub>2.5</sub> bias averaged over July 2018 at AQS sites is reduced at 64% of the

640 sites and the mean error is reduced at 77% of the sites. In areas where the BASE PM<sub>2.5</sub>

641 concentrations are biased high such as the Great Lakes region, most of the sites in the

642 east, and the west coast, the NEW model reduces bias and error. In areas where the  
 643 BASE model was low, such as Texas and the southern plains, the bias is slightly  
 644 increased although mean absolute error is less affected. In these areas the difference in  
 645 dry deposition velocity is relatively small because there is less vegetation and not much  
 646 forest. Note that the increased bias and error at some sites in SW Oregon and northern  
 647 CA are related to very high  $PM_{2.5}$  concentrations caused by wildfires.



648  
 649 Figure 16. Evaluation of modeled hourly  $PM_{2.5}$  compared to AQS measurements  
 650 averaged for July 2018: (a) NEW – BASE absolute bias difference, and (b) NEW –  
 651 BASE mean absolute error difference.

652

## 653 **6. Conclusions and future work**

654 The modeling of dry deposition in general, and aerosol dry deposition in particular,  
 655 contribute large amounts of uncertainty to air quality and climate models (e.g., Solazzo et  
 656 al., 2012; Mahowald et al., 2017). Thus, improving the mechanistic underpinnings of dry  
 657 deposition calculations helps improve accuracy of the modeling systems. The new  
 658 development to the aerosol dry deposition model was driven by the aggregation of  
 659 experimental data showing that existing models are unable to accurately replicate the  
 660 observed relationship between particle size and dry deposition velocity especially for  
 661 forested areas. Since the quasi-laminar sublayer resistance  $R_b$  is usually the controlling

662 resistance during peak deposition conditions (daytime), the new developments focus on  
663 revision of the  $R_b$  parameterizations, particularly the impaction efficiency. The  
664 development process was to revise the impaction efficiency to get better agreement with  
665 the aggregate measurements while maintaining physically plausible rationales. The key  
666 innovation was to add a second term to the impaction efficiency (equation 7) that  
667 represents impaction on microscale obstacles. For broadleaf vegetation the concept is  
668 that many species have leaf hairs or other microscale roughness features. However,  
669 needleleaf species generally do not have hairs but they may have ridges or other  
670 microscale obstacles. Since experimental studies have found that needleleaf species have  
671 high aerosol deposition rates, it is theorized that the needle shape itself may be a key  
672 factor as discussed in section 5.

673

674 The main impact of the new model is to increase dry deposition velocity in the  
675 accumulation size range. This has a large effect on  $PM_{2.5}$  especially in forested areas  
676 where the dry deposition velocity of accumulation mode mass can increase up to an order  
677 of magnitude compared to the current model in CMAQv5.3. For the high-resolution  
678 model application to the LISTOS the new model reduced  $PM_{2.5}$  concentration up to 40%  
679 downwind of NYC in CT for the case shown in Figure 11. For these applications in  
680 summer of 2018 where the BASE model generally overestimates  $PM_{2.5}$ , the NEW model  
681 which has much greater accumulation mode mass dry deposition, results in mostly better  
682 agreement with observations. However, aerosol concentrations are very difficult to  
683 model accurately not just because of uncertainties in dry deposition but also uncertainties

684 in emissions, transport and diffusion, wet scavenging, and very complex chemistry which  
685 involves semi-volatile organic and inorganic species (Appel et al., 2021).

686

687 Continued research on aerosol dry deposition is needed. More field studies, especially  
688 for some of the lesser studied vegetation land use types such as croplands, grasslands, and  
689 broadleaf deciduous forests, would help to confirm or refute the new model paradigm for  
690 different vegetation types and help define parameters such as the macro and micro scale  
691 characteristic obstacle dimensions and scaling factors. In addition to comparisons to  
692 aggregates of measurements we also plan to model individual field studies in detail where  
693 the aerosol dry deposition model is driven by observed micrometeorology and canopy  
694 characteristics on an observational timestep basis (30 min or 1 hour).

695

696 Another next step in this research is to include the effects of brown vegetation in the  
697 model. Currently, the vegetation fraction and LAI are specified in the WRF-CMAQ  
698 system either by land-use category look-up table, where the parameters seasonally vary  
699 between minimum and maximum values, or from MODIS satellite fraction of absorbed  
700 photosynthetically active radiation (FPAR) and LAI retrievals. In either case, the  
701 vegetation parameters are meant to represent live vegetation for evapotranspiration and  
702 stomatal uptake of gaseous pollutants. However, for aerosol deposition, brown  
703 vegetation can also provide surfaces for deposition. Therefore, we are planning to  
704 include MODIS non-photosynthetic vegetation (NPV) and photosynthetic vegetation  
705 (PV) fractions in the aerosol dry deposition model. Preliminary tests show that the  
706 inclusion of NPV increases aerosol deposition over large areas of the western US.

707 Implementation of NPV has already been included for windblown dust emissions where  
708 NPV reduces dust emissions by shielding the soil surface from the wind (Huang and  
709 Foroutan 2021).

710

### 711 **Disclaimer**

712 Although this work was reviewed by EPA and approved for publication, it may not  
713 necessarily reflect official Agency policy. Mention of commercial products does not  
714 constitute endorsement by the Agency.

### 715 **Acknowledgments**

716 We gratefully acknowledge the free availability and use of observational data sets from  
717 EPA AQS (available at <https://www.epa.gov/aqs>). Data used to generate figures and  
718 tables shown in this article can be downloaded at

719 <https://edg.epa.gov/metadata/catalog/main/home.page>. We thank Christian Hogrefe and  
720 Chris Nolte for comments and suggestions on the initial version of this paper.

721

### 722 **References**

- 723 Ahlm, L., Krejci, R., Nilsson, E. D., Martensson, E. M., Vogt, M. and co-authors. 2010.  
724 Emission and dry deposition of accumulation mode particles in the Amazon  
725 Basin. *Atmos. Chem. Phys.* 10, 10237–10253. doi:10.5194/acp-10-10237-2010.
- 726 Albert, M. F., Anguelova, M. D., Manders, A. M., Schaap, M., & Leeuw, G. D. (2016).  
727 Parameterization of oceanic whitecap fraction based on satellite observations.  
728 *Atmospheric Chemistry and Physics*, **16**(21), pp.13725-13751.

- 729 Allen, A. G., Harrison, R. M. and Nicholson, K. W. 1991. Dry deposition of fine aerosol  
730 to a short grass surface. *Atmos. Environ.* 25A, 2671–2676.
- 731 Appel, K. W., Bash, J. O., Fahey, K. M., Foley, K. M., Gilliam, R. C., Hogrefe, C.,  
732 Hutzell, W. T., Kang, D., Mathur, R., Murphy, B. N., Napelenok, S. L., Nolte, C.  
733 G., Pleim, J. E., Pouliot, G. A., Pye, H. O. T., Ran, L., Roselle, S. J., Sarwar, G.,  
734 Schwede, D. B., Sidi, F. I., Spero, T. L., and Wong, D. C.: The Community  
735 Multiscale Air Quality (CMAQ) model versions 5.3 and 5.3.1: system updates  
736 and evaluation, *Geosci. Model Dev.*, 14, 2867–2897, [https://doi.org/10.5194/gmd-](https://doi.org/10.5194/gmd-14-2867-2021)  
737 [14-2867-2021](https://doi.org/10.5194/gmd-14-2867-2021), 2021.
- 738 Appel, K. W., Gilliam, R. C., Pleim, J. E., Pouliot, G. A., Wong, D. C., Hogrefe, C., et al.  
739 598 (2014). Improvements to the WRF-CMAQ modeling system for fine-scale air  
740 quality 599 simulations. *EM: Air and Waste Management Association's*  
741 *Magazine for Environmental 600 Managers* (September).
- 742 Beckett, K.P., Freer-Smith, P.H. and Taylor, G., 2000. Particulate pollution capture by  
743 urban trees: effect of species and windspeed. *Global change biology*, 6(8),  
744 pp.995-1003.
- 745 Beswick, K. M., Hargreaves, K. J., Gallagher, M. W., Choularton, T. W. and Fowler, D.  
746 1991. Size-resolved measurements of cloud droplet deposition velocity to a forest  
747 canopy using an eddy correlation technique. *Q. J. R. Met. Soc.* 117, 623–645.  
748 doi:10.1002/qj.49711749910.
- 749 Bey, I., D. J. Jacob, R. M. Yantosca, J. A. Logan, B. Field, A. M. Fiore, Q. Li, H. Liu, L.  
750 J. Mickley, and M. Schultz, Global modeling of tropospheric chemistry with

- 751 assimilated meteorology: Model description and evaluation, *J. Geophys. Res.*,  
752 106, 23,073-23,096, 2001.
- 753 Binkowski, F. S. & Shankar, U. (1995). The regional particulate matter model: 1. Model  
754 description and preliminary results. *Journal of Geophysical Research:*  
755 *Atmospheres*, **100**(D12), pp.26191-26209.
- 756 Buzorius, G., Rannik, U., Makela, J. M., Keronen, P., Vesala, T. and co-authors. 2000.  
757 Vertical aerosol fluxes measured by the eddy covariance method and deposition  
758 of nucleation mode particles above a Scots pine forest in southern Finland. *J.*  
759 *Geophys. Res.* 105, 19905–19916.
- 760 Byun, D., & Schere, K. L. (2006). Review of the governing equations, computational  
761 algorithms, and other components of the models-3 Community Multiscale Air  
762 Quality (CMAQ) modeling system. *Applied Mechanics Reviews*, 59(1–6).  
763 <https://doi.org/10.1115/1.2128636>
- 764 Caffrey, P. F., Ondov, J. M., Zufall, M. J. and Davidson, C. I. 1998. Determination of  
765 size-dependent dry particle deposition velocities with multiple intrinsic elemental  
766 tracers. *Environ. Sci. Technol.* 32, 1615–1622. doi:10.1021/es970644f.
- 767 Chamberlain, A. C. 1967. Transport of Lycopodium spores and other small particles to  
768 rough surfaces. *Proceedings of the Royal Society of London* 296A, 45–70.
- 769 Chen, L., Liu, C., Zhang, L., Zou, R., & Zhang, Z. (2017). Variation in tree species  
770 ability to capture and retain airborne fine particulate matter (PM 2.5). *Scientific*  
771 *Reports*, **7**(1), pp.1-11.

- 772 Chiam, Z., Song, X. P., Lai, H. R., & Tan, H. T. W. (2019). Particulate matter mitigation  
773 via plants: Understanding complex relationships with leaf traits. *Science of the*  
774 *total environment*, **688**, pp.398-408
- 775 Clough, W. S. 1975. The deposition of particles on moss and grass surfaces. *Atmos.*  
776 *Environ.* 9, 1113–1119. doi:10.1016/0004-6981(75)90187-0.
- 777 Connan O, Pellerin G, Maro D, Damay P, Hébert D, et al. 2018. Dry deposition velocities  
778 of particles on grass: field experimental data and comparison with models. *J.*  
779 *Aerosol Sci.* 126:58–67
- 780 Cunningham, E., 1910. On the velocity of steady fall of spherical particles through fluid  
781 medium. *Proc. Roy. Soc. A* 83, 357.
- 782 Deventer, M.J., Held, A., El-Madany, T.S. and Klemm, O., 2015. Size-resolved eddy  
783 covariance fluxes of nucleation to accumulation mode aerosol particles over a  
784 coniferous forest. *Agricultural and Forest Meteorology*, 214, pp.328-340.
- 785 Emerson, E. W., Hodshire, A. L., DeBolt, H. M., Billsback, K. R., Pierce, J. R.,  
786 McMeeking, G. R., & Farmer, D. K. (2020). Revisiting particle dry deposition  
787 and its role in radiative effect estimates. *Proceedings of the National Academy of*  
788 *Sciences*, **117**(42), pp.26076-26082.
- 789 ENVIRON. 2020. User's Guide, Comprehensive Air Quality Model with Extensions  
790 (CAMx), Version 7.10. [https://camx-](https://camx-wp.azurewebsites.net/Files/CAMxUsersGuide_v7.10.pdf)  
791 [wp.azurewebsites.net/Files/CAMxUsersGuide\\_v7.10.pdf](https://camx-wp.azurewebsites.net/Files/CAMxUsersGuide_v7.10.pdf).
- 792 Farmer, D. K., Boedicker, E. K., & DeBolt, H. M. (2021). Dry Deposition of  
793 Atmospheric Aerosols: Approaches, Observations, and Mechanisms. *Annual*  
794 *Review of Physical Chemistry*, **72**, pp.375-397.

- 795 Gallagher, M. W., Choulaton, T. W., Morse, A. P. and Fowler, D. 1988. Measurements  
796 of the size dependence of cloud droplet deposition at a hill site. *Q. J. R. Meteorol.*  
797 *Soc.* 114, 1291–1303.
- 798 Gallagher, M. W., Beswick, K. M., Duyzer, J., Westrate, H., Choulaton, T. W. and co-  
799 authors. 1997. Measurements of aerosol fluxes to Speulder Forest using a  
800 micrometeorological technique. *Atmos. Environ.* 31, 359–373.
- 801 Gaman, A., Rannik, U., Aalto, P., Pohja, T., Siivola, E. and coauthors. 2004. Relaxed  
802 eddy accumulation system for size resolved aerosol particle flux measurements. *J.*  
803 *Atmos. Oceanic Technol.* 21, 933–943.
- 804 Gong, W., Dastoor, A.P., Bouchet, V.S., Gong, S., Makar, P.A., Moran, M.D., Pabla, B.,  
805 Ménard, S., Crevier, L.P., Cousineau, S. and Venkatesh, S., 2006. Cloud  
806 processing of gases and aerosols in a regional air quality model (AURAMS).  
807 *Atmospheric Research*, 82(1-2), pp.248-275.
- 808 Gong, W., Makar, P.A., Zhang, J., Milbrandt, J., Gravel, S., Hayden, K.L., Macdonald,  
809 A.M. and Leaitch, W.R., 2015. Modelling aerosol–cloud–meteorology  
810 interaction: A case study with a fully coupled air quality model (GEM-MACH).  
811 *Atmospheric Environment*, 115, pp.695-715.
- 812 Gordon, M., Staebler, R. M., Liggio, J., Vlasenko, A., Li, S.-M. and co-authors. 2011.  
813 Aerosol flux measurements above a mixed forest at Borden, Ontario. *Atmos.*  
814 *Chem. Phys.* 11, 6773–6786.
- 815 Grönholm, T., Aalto, P. P., Hiltunen, V., Rannik, U., Rinne, J. and co-authors. 2007.  
816 Measurements of aerosol particle dry deposition velocity using the relaxed eddy  
817 accumulation technique. *Tellus* 59B, 381–386.

- 818 Grönholm, T., Launiainen, S., Ahlm, L., Martensson, E. M., Kulmala, M. and co-authors.  
819 2009. Aerosol particle dry deposition to canopy and forest floor measured by two-  
820 layer eddy covariance system. *J. Geophys. Res.* 114, D04202.  
821 doi:1029/2008JD010663.
- 822 Grosch, S. and Schmitt, G. 1988. Experimental Investigations on the Deposition of Trace  
823 Elements in Forest Area. In: *Environmental Meteorology* (eds. K. Grefen and L.  
824 Lobel). Kluwer Academic Publishers, Dordrecht, The Netherlands, pp. 201–216.
- 825 Hicks, B. B., Wesely, M. L., Durham, J. L. and Brown, M. A. 1982. Some direct  
826 measurements of atmospheric sulfur fluxes over a pine plantation. *Atmos.*  
827 *Environ.* 16, 2899–2903.
- 828 Hicks, B. B., Matt, D. R., McMillen, R. T., Womack, J. D., Wesely, M. L. and co-  
829 authors. 1989. A field investigation of sulfate fluxes to a deciduous forest. *J.*  
830 *Geophys. Res.* 94, 13003–13011.
- 831 Hofken, K. D. and Gravenhorst, G. 1982. Deposition of atmospheric aerosol particles to  
832 beech- and spruce forest. In: *Deposition of Atmospheric Pollutants* (eds. H. W.  
833 Georggi and J. Pankrath). D. Reidel Publishing Company, Oberursel/Taunus,  
834 Germany, pp. 191–194.
- 835 Huang, X. and Foroutan, H., 2021. Effects of Non-Photosynthetic Vegetation on Dust  
836 Emissions. *Earth and Space Science Open Archive ESSOAr*.
- 837 Hummelshøj, P. N. O. S. E., Jensen, N. O., & Larsen, S. E. (1992). Particle dry  
838 deposition to a sea surface. Precipitation scavenging and atmosphere-surface  
839 exchange, *Hemisphere Publishing Corporation, Washington*, **5562**, pp.829-840.

- 840 Hummelshøj, P. 1994. Dry Deposition of Particles and Gases. PhD Thesis, Technical  
841 University of Denmark.
- 842 IPCC, 2021: Climate Change 2021: The Physical Science Basis. Contribution of Working  
843 Group I to the Sixth Assessment Report of the Intergovernmental Panel on  
844 Climate Change [Masson-Delmotte, V., P. Zhai, A. Pirani, S.L. Connors, C. Péan,  
845 S. Berger, N. Caud, Y. Chen, L. Goldfarb, M.I. Gomis, M. Huang, K. Leitzell, E.  
846 Lonnoy, J.B.R. Matthews, T.K. Maycock, T. Waterfield, O. Yelekçi, R. Yu, and  
847 B. Zhou (eds.)]. Cambridge University Press. In Press.
- 848 Karambelas, A., LISTOS: Toward a Better Understanding of New York City's Ozone  
849 Pollution Problem, EM, October 2020.
- 850 Lavi, A., Farmer, D. K., Segre, E., Moise, T., Rotenberg, E. and co-authors. 2013. Fluxes  
851 of fine particles over a semi-arid pine forest: Possible effects of a complex terrain.  
852 *Aerosol. Sci. Technol.* 47, 906–915.
- 853 Leonard, R.J., McArthur, C. and Hochuli, D.F., 2016. Particulate matter deposition on  
854 roadside plants and the importance of leaf trait combinations. *Urban Forestry &*  
855 *Urban Greening*, 20, pp.249-253.
- 856 Lorenz, R. and Murphy, C. E. Jr. 1989. Dry deposition of particles to a pine plantation.  
857 *Boundary-Layer Meteorol.* 46, 355–366.
- 858 Mahowald, N.M., Scanza, R., Brahney, J. et al. Aerosol Deposition Impacts on Land and  
859 Ocean Carbon Cycles. *Curr Clim Change Rep* 3, 16–31 (2017).  
860 <https://doi.org/10.1007/s40641-017-0056-z>

- 861 Mammarella, I., Rannik, U., Aalto, P., Keronen, P., Vesala, T. and co-authors. 2011.  
862 Long-term aerosol particle flux observations. Part II: Particle size statistics and  
863 deposition velocities. *Atmos. Environ.* 45, 3794–3805.
- 864 Matsuda, K., Watanabe, I., Mizukami, K., Ban, S. and Takahashi, A. 2015. Dry  
865 deposition of PM<sub>2.5</sub> sulfate above a hilly forest using relaxed eddy accumulation.  
866 *Atmos. Environ.* 107, 255–261.
- 867 Moller, U. and Schumann, G. 1970. Mechanisms of transport from the atmosphere to the  
868 Earth's surface. *J. Geophys. Res.* 75, 3013–3019.
- 869 Nemitz, E., Gallagher, M. W., Duyzer, J. H. and Fowler, D. 2002. Micrometeorological  
870 measurements of particle deposition velocities to moorland vegetation. *Q. J. R.*  
871 *Meteorol. Soc.* 128, 2281–2300.
- 872 Neumann, H. H. and den Hartog, G. 1985. Eddy correlation measurements of  
873 atmospheric fluxes of ozone, sulphur, and particulates during the Champaign  
874 Intercomparison Study. *J. Geophys. Res.* 90, 2097–2110.
- 875 Ould-Dada, Z. 2002. Dry deposition profile of small particles within a model spruce  
876 canopy. *Sci. Total Environ.* 286, 83–96.
- 877 Pleim, J. and Ran, L. 2011. Surface flux modeling for air quality applications.  
878 *Atmosphere* 2, 271–302.
- 879 Perini, K., Ottel , M., Giulini, S., Magliocco, A. and Roccotiello, E., 2017.  
880 Quantification of fine dust deposition on different plant species in a vertical  
881 greening system. *Ecological engineering*, 100, pp.268-276.

- 882 Petroff, A. and Zhang, L. 2010. Development and validation of a size-resolved particle  
883 dry deposition scheme for application in aerosol transport models. *Geosci. Model*  
884 *Dev.* 3, 753–769.
- 885 Petroff, A., Murphy, J.G., Thomas, S.C. and Geddes, J.A., 2018. Size-resolved aerosol  
886 fluxes above a temperate broadleaf forest. *Atmospheric Environment*, 190,  
887 pp.359-375.
- 888 Pryor, S. C., Barthelmie, R. J., Geernaert, L. L. S., Ellermann, T., & Perry, K. D. (1999).  
889 Speciated particle dry deposition to the sea surface: results from ASEPS'97.  
890 *Atmospheric Environment*, **33**(13), pp.2045-2058.
- 891 Pryor, S. C. 2006. Size-resolved particle deposition velocities of sub-100nm diameter  
892 particles over a forest. *Atmos. Environ.* 40, 6192–6200.
- 893 Pryor, S.C., Larsen, S.E., Sørensen, L.L., Barthelmie, R.J., Grönholm, T. and co-authors.  
894 2007. Particle fluxes over forests: analyses of flux methods and functional  
895 dependencies. *J. Geophys. Res.: Atmos.*, 112, D07205,  
896 doi:10.1029/2006JD008066.
- 897 Pryor, S.C., Gallagher, M., Sievering, H., Larsen, S.E., Barthelmie, R.J., Birsan, F.,  
898 Nemitz, E., Rinne, J., Kulmala, M., Grönholm, T. and Taipale, R., 2008. A review  
899 of measurement and modelling results of particle atmosphere–surface exchange.  
900 *Tellus B: Chemical and Physical Meteorology*, 60(1), pp.42-75.
- 901 Pryor, S. C., Barthelmie, R. J., Spaulding, A. M., Larsen, S. E., and Petroff, A. (2009).  
902 Size-Resolved Aerosol Particle Fluxes over Forests. *J. Geophys. Res.*, 114,  
903 doi:10.1029/2009JD012248.

- 904 Sæbø, A., Popek, R., Nawrot, B., Hanslin, H.M., Gawronska, H., Gawronski, S.W., 2012.  
905 Plant species differences in particulate matter accumulation on leaf surfaces. *Sci.*  
906 *Total Environ.* 427 (-428), 347–354,  
907 <http://dx.doi.org/10.1016/j.scitotenv.2012.03.084>.
- 908 Saylor, R. D., Baker, B. D., Lee, P., Tong, D., Pan, L., & Hicks, B. B. (2019). The  
909 particle dry deposition component of total deposition from air quality models:  
910 right, wrong or uncertain?. *Tellus B: Chemical and Physical Meteorology*, **71**(1),  
911 p.1550324.
- 912 Sievering, H. 1981. Profile measurements of particle mass transfer at the air-water  
913 interface. *Atmos. Environ.* 15, 123–129.
- 914 Sievering, H. 1982. Profile measurements of particle dry deposition velocity at an air-  
915 land interface. *Atmos. Environ.* 16, 301–306.
- 916 Sievering, H. 1988. Small-particle dry deposition measurements: A comparison of  
917 gradient and eddy flux techniques over agricultural fields, In: Annual Meeting of  
918 Air Pollution Control Association, Dallas, Texas, June 19–24, 6, pp. 88–101.
- 919 Slinn, W. G. N. 1977. Some approximations for the wet and dry removal of particles and  
920 gases from the atmosphere. *Water Air Soil Pollut.* 7, 513–543.
- 921 Slinn, S. A. & Slinn, W. G. N. (1980). Predictions for particle deposition on natural  
922 waters. *Atmospheric Environment (1967)*, **14**(9), pp.1013-1016.
- 923 Slinn, W. G. N. (1982). Predictions for particle deposition to vegetative canopies.  
924 *Atmospheric Environment (1967)*, **16**(7), pp.1785-1794.
- 925 Solazzo, E., Bianconi, R., Pirovano, G., Matthias, V., Vautard, R., Moran, M.D., Appel,  
926 K.W., Bessagnet, B., Brandt, J., Christensen, J.H. and Chemel, C., 2012.

- 927 Operational model evaluation for particulate matter in Europe and North America  
928 in the context of AQMEII. *Atmospheric environment*, **53**, pp.75-92.
- 929 Stokes, G. G. 1851. On the effect of internal friction of fluids on the motion of  
930 pendulums. *Transactions of the Cambridge Philosophical Society*. 9, part ii: 8–  
931 106.
- 932 Sun, F., Yin, Z., Lun, X., Zhao, Y., Li, R. and co-authors. 2014. Deposition velocity of  
933 PM2.5 in the winter and spring above deciduous and coniferous forests in Beijing,  
934 China. *PLoS One* 9, e97723. doi: 10.1371/journal.pone.0097723.
- 935 Torres-Vazquez, A., Pleim, J., Gilliam, R., Pouliot, G., 2022, Performance Evaluation of  
936 the Meteorology and Air Quality Conditions from 1 Multiscale WRF CMAQ  
937 Simulations for the Long Island Sound Tropospheric 2 Ozone Study (LISTOS),  
938 submitted to *Journal of Geophysical Research: Atmospheres*
- 939 Toro, C., Foley, K., Simon, H., Henderson, B., Baker, K.R., Eyth, A., Timin, B., Appel,  
940 W., Luecken, D., Beardsley, M. and Sonntag, D., 2021. Evaluation of 15 years of  
941 modeled atmospheric oxidized nitrogen compounds across the contiguous United  
942 States. *Elem Sci Anth*, 9(1), p.00158.
- 943 Venkatram, A. and Pleim, J. 1999. The electrical analogy does not apply to modeling dry  
944 deposition of particles. *Atmos. Environ.* 33, 3075–3076.
- 945 Vong, R. J., Vong, I. J., Vickers, D. and Covert, D. S. 2010. Size-dependent aerosol  
946 deposition velocities during BEARPEX'07. *Atmos. Chem. Phys.* 10, 5749–5758.
- 947 Vong, R. J., Vickers, D. and Covert, D. S. 2004. Eddy correlation measurements of  
948 aerosol deposition to grass. *Tellus* 56B, 105–117.

- 949 Waraghai, A. and Gravenhorst, G. 1989. Dry deposition of atmospheric particles to an  
950 old spruce stand, in: *Mechanisms and Effects of Pollutant Transfer into Forests*.  
951 (ed. H. W. Georgii), Kluwer Academic Publishers, London, pp. 77–86.
- 952 Weerakkody, U., Dover, J. W., Mitchell, P., & Reiling, K. (2018). Evaluating the impact  
953 of individual leaf traits on atmospheric particulate matter accumulation using  
954 natural and synthetic leaves. *Urban forestry & urban greening*, **30**, pp.98-107.
- 955 Wesely, M. L., Hicks, B. B., Dannevik, W. P., Frisella, S. and Husar, R. B. 1977. An  
956 eddy-correlation measurement of particulate deposition from the atmosphere.  
957 *Atmos. Environ.* 11, 561–563.
- 958 Wesely, M. L., Cook, D. R., Hart, R. L. and Speer, R. E. 1985. Measurements and  
959 parameterization of particulate sulfur dry deposition over grass. *J. Geophys. Res.*  
960 90, 2131–2143.
- 961 Wyers, G. P. and Duyzer, J. H. 1997. Micrometeorological measurement of the dry  
962 deposition flux of sulphate and nitrate aerosols to coniferous forest. *Atmos.*  
963 *Environ.* 31, 333–343.
- 964 Zhang, L., Gong, S., Padro, J., & Barrie, L. (2001). A size-segregated particle dry  
965 deposition scheme for an atmospheric aerosol module. *Atmospheric environment*,  
966 **35**(3), pp.549-560.
- 967 Zhang, J. and Shao, Y., 2014. A new parameterization of particle dry deposition over  
968 rough surfaces. *Atmospheric Chemistry and Physics*, 14(22), pp.12429-12440.
- 969 Zhang, J., Shao, Y. and Huang, N. 2014. Measurements of dust deposition velocity in a  
970 wind-tunnel experiment. *Atmos. Chem. Phys.* 14, 8869–8882.

- 971 Zufall, M. J., Davidson, C. I., Caffrey, P. F. and Ondov, J. M. 1998. Airborne  
972 concentrations and dry deposition fluxes of particulate species to surrogate  
973 surfaces deployed in southern Lake Michigan. *Environ. Sci. Technol.* 32, 1623–  
974 1628.
- 975 Zhang, X., Lyu, J., Zeng, Y., Sun, N., Liu, C. and Yin, S., 2021. Individual effects of  
976 trichomes and leaf morphology on PM<sub>2.5</sub> dry deposition velocity: A variable-  
977 control approach using species from the same family or genus. *Environmental*  
978 *Pollution*, 272, p.116385.